EPJ Web of Conferences **87**, 02011 (2015)
DOI: 10.1051/epjconf/20158702011

Recent Upgrading of ECRH System and Studies to Improve ECRH Performance in the LHD

Hiroe Igami[1,a], Shin Kubo[1], Takashi Shimozuma[1], Yasuo Yoshimura[1], Hiromi Takahashi[1], Shuji Kamio[1], Sakuji Kobayashi[1], Satoshi Ito[1], Yoshinori Mizuno[1], Kohta Okada[1], Ryohei Makino[2], Shinya Ogasawara[2], Kenya Kobayashi[2], Masaki Osakabe[1], Kazunobu Nagasaki[3], Hiroshi Idei[4], Takashi Mutoh[1] and LHD experiment group

[1] National Institute for Fusion Science, Toki, 509-5292, Japan
[2] Department of Energy Engineering and Science, Nagoya University Nagoya, 464-8603, Japan
[3] Institute of Advanced Energy, Kyoto University 611-0011 Uji, Japan
[4] Research Institute for Applied Mechanics, Kyushu University 816-8580 Kasuga, Japan

Abstract. This paper reports the recent status of the ECRH system in the LHD and introduces the experimental results that suggest the reasonable effects of the wave-plasma interaction in the plasma boundary including outside the LCFS. With increasing the available ECRH power, ECRH/ECCD have been performed in higher density target plasmas where the mode coupling between the O-mode and the X-mode caused by the magnetic shear occurs for long distance in the low density region of the plasma boundary including the ergodic layer outside the LCFS. In such a case, the incident polarization should be set by taking into account the mode coupling effect. Moreover, the refraction in the boundary region should be considered for accurate numerical prediction of the wave trajectory and power absorption with use of the ray-tracing calculation.

1 Introduction

In the Large Helical Device (LHD), the electron cyclotron resonance heating (ECRH) system has been developed and upgraded with increasing the input power and the pulse length. Since 2007, three 77 GHz (~1 MW / 5 s and 0.3 MW/CW) and one 154 GHz (1 MW / 5 s and 0.5 MW/CW) triode CPD gyorotrons developed in collaboration with Tsukuba University and fabricated by TOSHIBA, have been installed continuously [1].

It is important to optimize the launching condition to obtain high heating efficiency. However, after one *154 GHz* gyrotron was installed in 2012, in a relatively high density plasma where the central electron density is about 2 x 10^{19} m^{-3}, it was found that the ECRH efficiency of the 77 GHz electron cyclotron (EC) wave is about 60% that is 30-40% less than that of 154 GHz EC wave which is almost 100% estimated in the same ways even if the ray-tracing calculation suggests 100% power absorption in both cases [2]. On the contrary, in the previous study in the LHD, it was shown that almost all of the injected power was absorbed for 82.7 GHz and 84 GHz EC waves by adjusting incident wave polarization [3] in low density plasmas where the line averaged electron density $\tilde{n}_e$ was about 0.5 x 10^{19} m^{-3}. Recently we have obtained helpful experimental results to consider this problem. The results suggest that the mode coupling between the O-mode and the X-mode caused by the existence of the magnetic shear [4] takes places in the low density region in the plasma boundary including the ergodic layer that surrounds the last closed flux surface (LCFS). It can be speculated that the power fraction of the incident wave that finally couples with the propagating mode used for ECRH (heating mode) is reduced by this mode coupling effect.

In addition to the mode coupling effect, the refraction of the wave in the low density boundary region including the ergodic layer may have to be taken into account to predict the wave propagation and the power deposition accurately by ray-tracing. In the LHD, a transmitted beam pattern monitor constructed of a carbon target plate and an infrared camera is installed in a lower port that is placed on the opposite side of the ECRH antenna installed in an upper port [5]. We have compared the experimentally observed beam pattern on the target plate with those obtained by multi ray-tracing for various start/end points of different densities. From this comparison it can be suggested that the refraction of the wave in the boundary region also should be taken into account for precise control of the wave trajectory.

In this paper, we first report the recent status of the ECRH system in the LHD in Section 2. In Section 3, the reduction of the ECRH efficiency of the right handed circular (R-circ) wave although the absolute value of the component of the refractive index parallel to the magnetic field ($|N_{//}|$) is large enough that the X-mode fraction of the

[a] Corresponding author: igami@LHD.nifs.ac.jp

R-circ. wave at the LCFS is high will be reported. In Section 4, comparison of the transmitted beam pattern on the target plate observed in the experiment with those predicted by multi ray-tracing for the cases of different densities of the calculation start/end point will be introduced. We will summarize the contents in Section 5.

2 Recent ECRH System in the LHD

In the latest experimental campaign in 2013, one 82.7 GHz/ 0.5 MW/ 2 s non CPD (GYCOM) and one 84 GHz CPD (GYCOM) 0.2 MW/CW, three 77 GHz and one 154 GHz are operated for the experiments. The 77 *GHz* and 154 GHz gyrotrons were developed under collaboration with University of Tsukuba and fabricated by TOSHIBA. Their specifications and achieved operations are listed in table 1. With two steps rise of the anode voltage V_A to avoid the charge neutralization, higher output power can be achieved [1]. The performance of the CW operation has been improved via replacing a part of the body-collector DC break to low-loss Si_3N_4, improving the designs of the cavity, the launcher, and the phase correcting mirrors and introducing a relief window of the diffracted stray radiation inside the tube.

Table 1. Specification of 1MW gyrotrons and achieved operations (power injection into the dummy load)

Tube No.	Spec.	Pulse Operation < 5 s	CW Operation
77GHz #1R	1 MW/ 5 s 0.3 MW/ CW	1.01 MW/ 5 s (33.0%)	0.13 MW/935 s (21.7%)
	Two step V_A rise	1.41 MW/ 0.2 s (51.1%)	
77GHz #2(R)	1.2 MW/ 5s 0.3 MW/ CW	1.02 MW/ 5 s (30.3%)	*0.24 MW/1800 s (30.8%) *0.3MW/300s (31.3%)
	Two step V_A rise	1.30 MW/ 0.45 s (43.8%)	
77GHz #3(R)	1.5 MW/ 2 s 1.2 MW/ 10 s 0.3 MW/ CW	1.53 MW/1.6 s (36.0%)	*0.30MW/1800s (34.2%)
	Two step V_A rise	1.87 MW/ 0.1 s (37.2%) 1.78 MW/ 1 s (37.9%)	
154GHz #1 R	1.0MW/2s 0.5MW/CW	1.105MW/short (27%)	0.35MW/1800s (39.1%)
	Two step V_A rise	1.16MW/1.0s (36.9%)	

*Output power of the improved tubes

The output powers of the three 77 GHz and one 154 GHz gyrotrons are transmitted via 88.9 mm diameter evacuated corrugated waveguide systems. Two of the transmission lines for 77 GHz are connected upper port antennas and two of them for 77 GHz/ 154 GHz are connected to horizontal port antennas. The output power of the 84 GHz 0.2 MW/CW gyrotron is transmitted via a 31.75 mm diameter evacuated corrugated waveguide system that is connected a lower port antenna. The output power of the 82.7 GHz gyrotron is transmitted via an 88.9 mm diameter non-evacuated corrugated waveguide system and launched from an upper port antenna. The total simultaneous input power is 4.5 MW at maximum for the pulse length less than 0.5 s. Although long pulse (> 300 s) operations more than 0.3 MW were achieved with use of the dummy load except for 77 GHz #1R gyrotron, in long pulse injection toward the plasma, the input power and pulse length are restricted because of the increase of the pressure inside the tubes. Under that restriction, with alternately switched operation of the two 77 GHz gyrotrons at 155 *kW* and 110 *kW* and continuous operation of the *84 GHz* gyrotron at 130 *kW,* a plasma where $\tilde{n}_e$ < 1.0 x 10^{19} m^{-3} and the central electron density T_{e0} ~ 1.7 keV was maintained for 30 minutes by 0.26 MW power injection in total.

3 ECRH Efficiencies for Different Transverse Distances in the Ergodic layer

In a horizontal port of the LHD, two antennas are installed for 77 GHz and 154 GHz ECRH. For each antenna, the toroidal injection angle can be set for a wide range, thus these antennas can be used for ECCD and the electron Bernstein wave (EBW) excitation via the O-X-B mode conversion process. However, the ECRH efficiency of the 77 GHz EC wave tends to be 30 % less than that of 154 GHz EC wave estimated in the same way for the same target plasma. To consider this problem, we have obtained helpful experimental results. Figure 1-(A) shows a schematic view of the injection of the 77 GHz EC wave in a magnetic configuration (R_{ax}, $|B_t|$)=(3.75 m, 1.375 T) where R_{ax} is the distance from the centre of the torus to the magnetic axis and B_t is the magnetic field strength there. The second harmonic 77 GHz / 1.055 MW EC wave was injected with 100 % / 25 Hz power modulation as the right-hand circular polarized (R-circ.) wave at various toroidal injection angles defined as shown in Figure 1-(A). In any cases of injection, the incident beam can access the second harmonic electron cyclotron resonance (ECR) layer. However, as shown in Figure 1-(B), the ECRH efficiency is reduced substantially in the case of (d). In this paper the ECRH efficiency is estimated with procedure explained in Appendix. To check the power absorption region, with use of the fast Fourier transform (FFT) analysis of the electron cyclotron emission (ECE) signals, profiles of the modulation amplitude and the phase delay corresponding to the power modulated ECRH (MECH) frequency are plotted in figures 2-(A), (B). In any cases of injection, the bottom of the phase delay and the peak of the modulation amplitude are located inside the normalized minor radius r_{eff}/a_{99} = 0.3, where r_{eff} is the effective minor radius and a_{99} means the effective minor radius inside which 99 % of the electron kinetic energy exists. Also as shown in Figure 2-(C), (D), increase of the electron temperature in the central region during EC wave injection was observed by Thomson scattering measurement. Therefore, we can confirm that the ECR layer in the central region can be aimed without misalignment of the launching antenna. Assuming that the vacuum/plasma interface where the

incident electromagnetic EC wave couples with the propagation modes in the plasma, those are the ordinary (O-) mode and the extraordinary (X-) mode located at the LCFS, and the modes never couple with each other inside the vacuum/plasma interface, we estimated the X-mode fraction of the R-circ. wave with use of the magnetic field vector at the LCFS and plotted the ECRH efficiencies again versus this X-mode fraction in Figure 3. Although for the cases of (a), (b), (d) and (e), the X-mode fraction is more than 90 % because $N_{//}$ at the LCFS is sufficiently large, the ECRH efficiency is reduced in the case of (d), where $N_{//}$ is the component of the refractive index parallel to the external magnetic field. In the previous study, it was suggested that the vacuum/plasma interface is located outside the LCFS [3] and the incident wave polarization should be set to match that of the heating to match with that determined at the actual plasma/vacuum interface outside the LCFS.

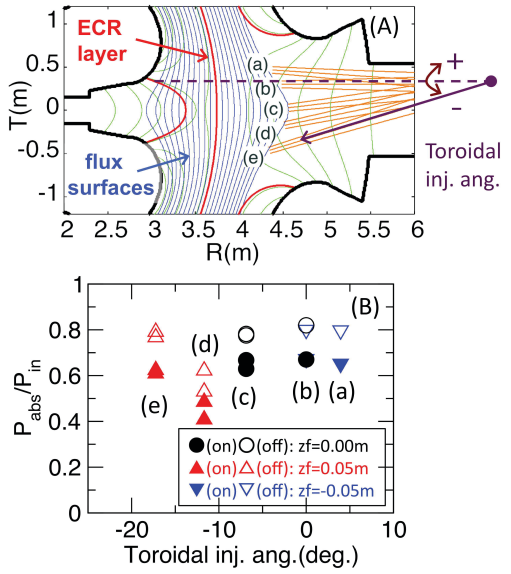

Figure 1: (A) Schematic view of the EC wave injection. (B) ECRH efficiencies estimated when ECRH is tuned on/off. Here, 'zf' is the vertical distance of the aiming point from the equatorial plane at R=3.9m.

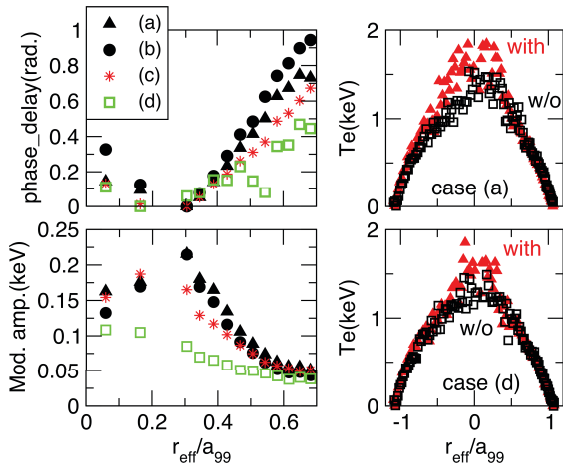

Figure 2: Profiles of the phase delay (A) and the modulation amplitude (B) corresponding to the MECH frequency (25Hz) for injection cases of (a)-(d) shown in Figure 1-(A). Profiles of the electron temperature with (triangle) and without (square) ECRH for the injection cases of (a) and (d).

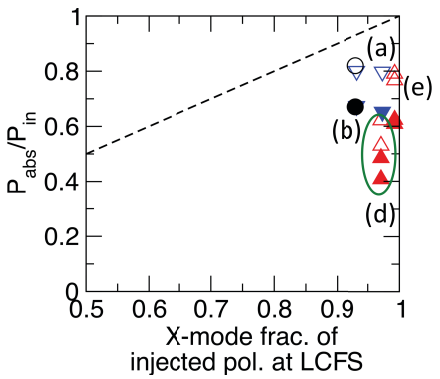

Figure 3: ECRH efficiencies for the injection cases of (a), (b), (d), and (e) plotted versus the X-mode fraction of the R-circ. wave with assuming that the vaccum/plasma interface is located at the LCFS.

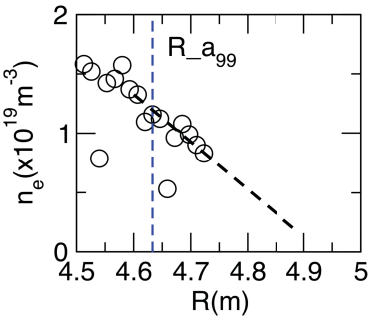

Figure 4: Radial profile of the electron density on the equatorial plane obtained by Thomson scattering measurement.

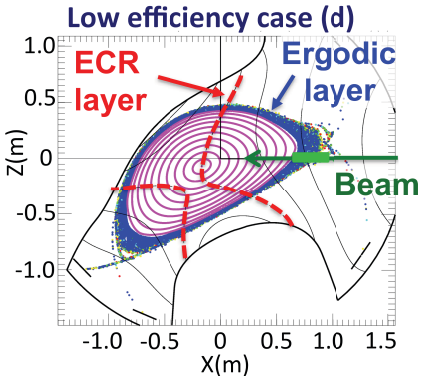

Figure 5: Cross-section view of the plasma along the incident beam for the case of injection (d).

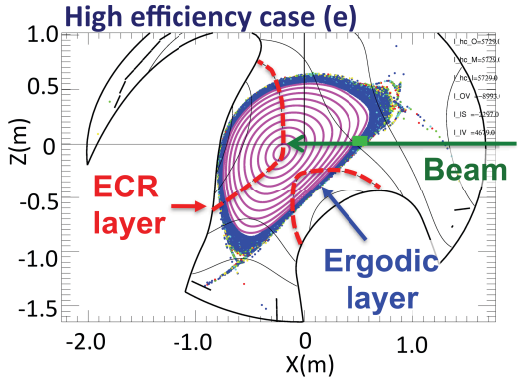

Figure 6: Cross-section view of the plasma along the incident beam for the case of injection (e).

Actually, in this experiment, the electron density exists outside the R_a_{99} where r_{eff}/a_{99} = 1.0 and seems to extend to the outside of the LCFS beyond R_a_{99} as shown in Figure 4, where R_a_{99} is the position of the a_{99} on the equatorial plane. We consider the LCFS is located at a_{99} for convenience. Figure 5 shows the cross-section view of the plasma along the incident beam for the injection case of (d). We can see that the ergodic layer where the plasma is weakly confined surrounds the LCFS. The transverse distance of the incident beam in the ergodic layer is about 0.3 m. However even if the vacuum/plasma interface is located 0.6 m beyond from the LCFS along the incident beam line, the X-mode fraction of the R-circ. wave remains more than 95 %. Therefore the reduce of the ECRH efficiency cannot be explained only by shift of the vacuum/plasma interface from the LCFS as long as we assume that the O-mode and the X-mode never couple with each other inside the vacuum/plasma interface.

One possible reason to explain this problem is the effect of the O-X mode coupling. For given magnetic field parameters B, θ, ϕ, and their gradients, there is a value of the electron density below which characteristic waves lose their identity [4] and the O-X mode coupling occurs. Here, B is the magnetic field strength, ϕ is the magnetic shear, θ is the angle between the magnetic field vector and the direction of the wave propagation z. If the transverse distance of such low density region is long enough, this effect of the O-X mode coupling cannot be ignored. Comparing with Figure 5 and Figure 6, the transverse distance in the ergodic layer is longer in the low efficiency case (d) than the high efficiency case (e). It can be speculated that in the low efficiency case (d), the transverse distance in the low density region with magnetic shear where the mode coupling takes place is long enough that the fraction of the injected power that finally couples with the X-mode that reaches the second harmonic ECR layer reduces.

An example of the 1-D full wave calculation along the straight injection beam of the 77GHz EC wave from the vacuum region to the plasma boundary [6] in a magnetic configuration (R_{ax}, B_t)=(3.60 m, -2.85 T) is given in figure 7. Profiles of the electron density n_e, and the angles θ, ϕ, defined above are plotted. The absolute value of the electric field components $|E_x|$ and $|E_y|$ perpendicular to the incident wave vector and the polarization parameters (α, β) change drastically more than the magnetic field line pitch in the hatched region. This result suggests the characteristics of the O- and the X-modes lose their identity in this region, although the fractions of the O- and the X- modes can be determined with assuming the uniform plasma at each point. In other words, this effect of the O-X mode coupling reduces the fraction of the power that finally couples with the O-mode deep into the plasma. In this calculation the electron density profile is given artificially, however, it is required to give the density profile corresponding to the reality to estimate the mode coupling effect accurately.

In any case, we have experimentally found the injection angles of the 77 GHz R-circ. EC wave to obtain more than 80 % ECRH efficiency as with the cases of (a), (b), and (e) shown in Figures 1-(A),(B). In a magnetic configuration (R_{ax}, B_t) = (3.60 m, -2.75 T), the ECRH efficiency of the 77 GHz and 154 GHz EC waves injected from the horizontal port antennas have been investigated for various target plasma densities. A fixed injection angle was adopted for 77 the GHz ECRH. With the injection angle, high ECRH efficiency was obtained in the configuration of (R_{ax}, $|B_t|$) = (3.75m, 1.375 T). Figure 8 shows that in the region where the electron density normalized by the cut-off density of the heating mode is less than 0.4, the ECRH efficiency of the 77 GHz EC wave remains more than 80 %.

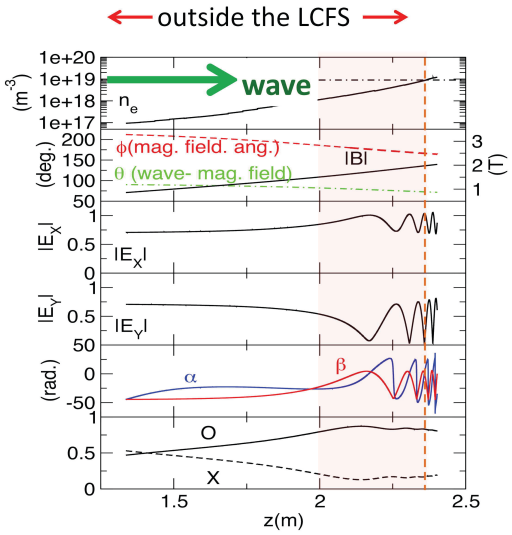

Figure 7: A result of 1-D full wave calculation in a magnetic field configuration (R_{ax}, B_t)=(3.60 m, -2.85 T). [Poster presentation by S. Kubo et al. in this conference]

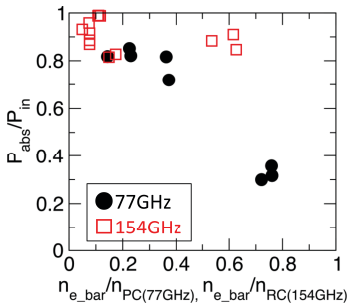

Figure 8: ECRH efficiencies of the 77 GHz (●) and 154 GHz (□) EC waves versus the line averaged density normalized by the cut-off density of each heating mode.

4 Difference of the Wave Trajectory for Different Start/end Points of the Ray-tracing Calculation

Adding to the mode coupling effect mentioned in the above section, we may have to take into account the effect of the refraction in the boundary region to predict the wave trajectory and the power absorption region accurately in the numerical analysis with ray-tracing. In the LHD, a transmitted beam pattern monitor constructed of a carbon target plate and an infrared camera is installed in a lower port that places on the opposite side of the EC wave launcher installed in an upper port [5]. We have

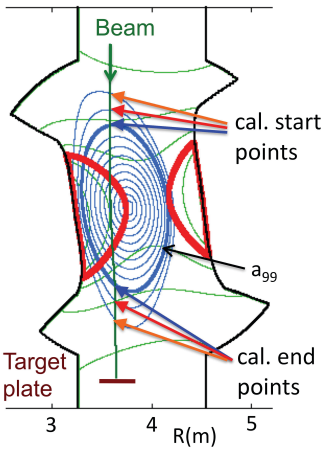

Figure 9: Schematic view of the EC wave injection toward the centre of the target plate through the plasma. Three types of the start/end points of the ray-tracing are selected on the points r_{eff}/a_{99} = 1.0, 1.1, 1.2 where the electron density is 0.76, 0.26, 0.01 x 10^{19} m^{-3} respectively.

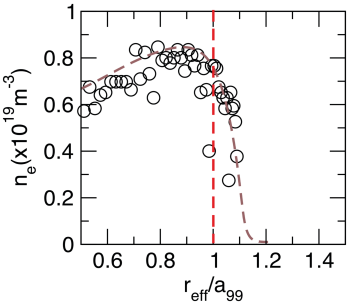

Figure 10: Electron density profile during the EC wave injection as shown in Figure 9. The fitted profile used in the ray-tracing is given by dashed line.

compared the experimentally observed beam pattern on the target plate with those obtained by multi ray-tracing for various start/end points of different densities in a magnetic configuration (R_{ax}, B_t)=(3.60 m, -0.95 T), where 77 GHz / 0.8 MW EC wave was injected for 0.2 s from the upper port antenna toward the centre of the target plate in the lower port. The schematic view of the experiment is given in Figure 9. In this launching condition, the predicted power absorption of the X-mode is about 10 % and most of the O-mode transmits through the plasma without absorption. The electron density profile measured in this experiment is shown in Figure 10. Also in this case, the electron density exist even in the region r_{eff}/a_{99} = 1 as shown in Figure 10. In the calculation the effective minor radius r_{eff} is given by interpolation of the meshed data partitioned every 2.0 degrees in the toroidal direction. This meshed data is provided for every time slices of the Thomson scattering measurement by mapping program to refer to the large-scale equilibrium database calculated with the VMEC code [7] and measured plasma parameters [8]. If a map position is outside the calculation boundary, id est the LCFS, given as an artificial input in the VMEC code, the corresponding r_{eff} is given by linear extrapolation technique as mentioned in section 3 in [8] to some extent. Therefore even in the point where $r_{eff}/a_{99} > 1$, the electron density can be given as a function of r_{eff}/a_{99} by fitting the

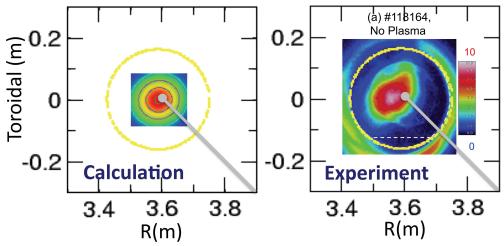

Figure 11: Beam pattern without the plasma obtained with multi ray-tracing (left) and in the experiment (right) [Poster presentation by H. Takahashi et al. in this conference].

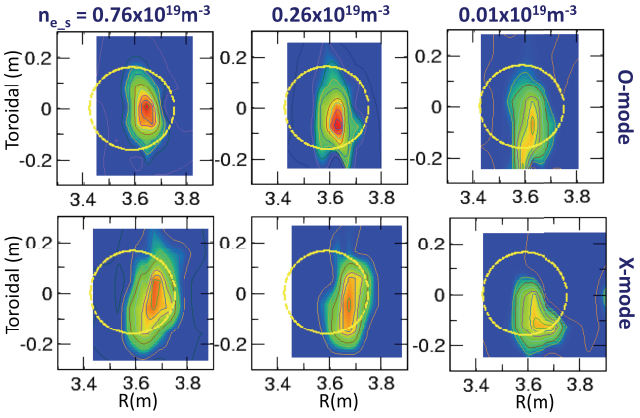

Figure 12: Beam patterns predicted by multi ray-tracing for different start/end points where the electron density is 0.76, 0.26, and 0.01 x 10^{19} m^{-3} respectively. Patterns of the pure O-mode (upper) and the pure X-mode (lower) are shown.

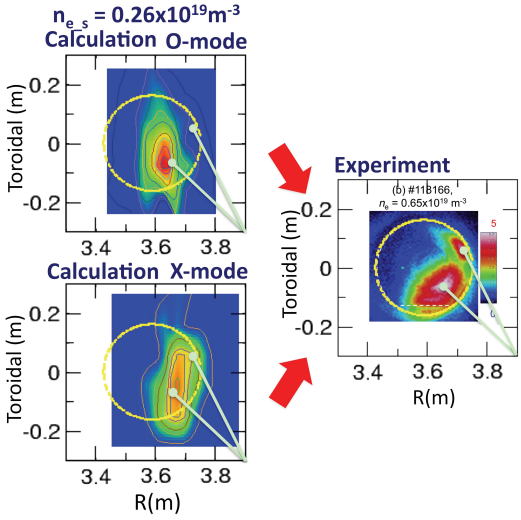

Figure 13: Beam patterns of the pure O-mode and X-mode predicted by multi ray-tracing for different start/end points where the electron density is 0.26 x 10^{19} m^{-3} and a transmitted beam pattern with a plasma obtained in the experiment [Poster presentation by H. Takahashi et. al, in this conference].

density profile obtained by Thomson scattering measurement as shown with a dashed line in Figure 10. The electron temperature profile is also given in the similar way.

Figure 11 shows the calculated and experimentally obtained [6] beam patterns without the plasma. We can confirm the alignment of the incident beam is good. To investigate the effect of the selection of the start/end

position, we performed multi ray-tracing calculations for three types of the start/end points r_{eff}/a_{99} = 1.0, 1.1, 1.2 as shown in figure 9 where n_{e_s} = 0.76, 0.26, and 0.01 x 10^{19} m^{-3} respectively as shown in figure 10. Figure 12 shows the difference of the beam patterns for each case. Both cases of the pure O-mode and the pure X-mode injection are calculated by multi ray-tracing with use of the fitted density profile as shown in figure 10. It can be seen that the beam patterns are expanded to the toroidal direction compared to the beam pattern without the plasma. In Figure 13, the experimental transmitted beam pattern is shown with calculated beam patterns of r_{eff}/a_{99} = 1.1 where n_{e_s} = 0.26 x 10^{19} m^{-3}. It seems that this experimentally obtained split beam pattern can be explained by summing the calculated beam patterns of the pure O-mode and the pure X-mode with adequate factors although the incident polarization was set to couple with the X-mode in reference to the previous study [3] where the experiment was performed in a lower density plasma. Similarly as discussed in the previous section, the mode coupling between the O- and the X-mode may also take place since the ergodic layer spreads widely along the long axis direction of the plasma cross section and the incident beam traverse long distance in the ergodic layer.

Here it has been derived that the multi ray-tracing started and ended based on Snell's law at the r_{eff}/a_{99} = 1 that corresponds to the LCFS where the electron density is 0.76 x 10^{19} m^{-3} cannot explain the experimentally obtained beam pattern even if both of the O-mode and the X-mode penetrates into the plasma as a result of the mode coupling effect. Generally in many ray-tracing codes, the calculation starts/ends at the LCFS and the wave vector is determined based on Snell's law. However, in many case the density at the LCFS is not zero and the plasma exists even outside the LCFS. In such cases, we have less accuracy of the ray-tracing.

3 Summary

In the LHD, the ECRH system has been developed for both purposes of high power and long pulse operations. As introduced in Section 2, the available total simultaneous input power is *4.5 MW* at maximum for the pulse length less than *0.5 s*. The performance of the CW operation has been improved via upgrading of the components of the gyrotron. However, the application to the long pulse discharge is restricted because of increase of the pressure inside the tubes.

After the installation of the 154 GHz gyrotron, it was derived that the 77 GHz ECRH efficiency tends to be less than that of 154 GHz. In Section 3, we reported helpful experimental results to consider this problem. When the incident wave traverses long distance in the low density region of the plasma boundary including the ergodic layer where the magnetic shear exists, the obtained ECRH efficiency is largely reduced. It can be speculated that the fraction of the incident power that finally couples with the heating mode is reduced because of the effect of the O-X mode coupling. To improve the ECRH efficiency in such a case, the incident polarization should be adjusted by taking into account the effect of the mode coupling in the boundary region. Adding to considering the mode coupling effect, as reported in section 4, the comparison between the experimentally obtained and the numerically predicted transmitted beam patterns through the plasma suggests that the refraction of the wave in the boundary region also should be taken into account. These results suggest the importance of the plasma modelling in the boundary region including outside the LCFS that has been neglected in the studies about the modelling of ECRH/ECCD in fusion oriented devices. Even in tokamaks, these issues should be considered if the EC wave is injected through the boundary stochastic region expanded by the RMP field for ELM mitigation to perform efficient ECRH/ECCD.

Appendix

The time derivative of the stored energy W_p is written as follows

$$\frac{dW_p}{dt} = \frac{W_p}{\tau_E} + P_{abs} + P_{other} - P_{rad}$$

where τ_E is the energy confinement time, P_{other} is the heating power except for the absorbed power of ECRH (P_{abs}), and P_{rad} is the radiation loss. If changes of τ_E, P_{rad} W_p, and P_{other} are negligibly small before (at $t=t_{before}$) and after (at $t=t_{after}$) ECRH is turned on/off, P_{abs} is obtained as follows.

$$\left| \frac{dW_p(t_{before})}{dt} - \frac{dW_p(t_{after})}{dt} \right| = P_{abs}$$

In this paper, the diamagnetic W_p signal is smoothed by conditional averaging during 25 Hz/100 % MECH and dW_p/dt is estimated by linear fitting of the smoothed signal. The ECRH efficiency, is obtained by dividing P_{abs} by the input power P_{inj} as P_{abs}/P_{inj}.

Acknowledgement

These works were mainly performed under the budget codes NIFS13ULRR701, 804

References

1. H. Takahashi, T. Shimozuma, S. Kubo et al. *AIP Conf. Proc.* ***1580*** pp.145 (2014)
2. R. Makino, S. Kubo, T. Ido et al. *JPS Conf. Proc.* **1**, pp. 015034(1-6) (2014)
3. T. Notake, S. Kubo, T. Shimozuma et al. Plasma Phys. Control. Fusion **47** pp. 531-544 (2005)
4. S. E. Segre, Plasma Phys. Control. Fusion **32** pp 1249-1254 (1990)
5. H. Takahashi et al. (Poster presentation in this conference)
6. S. Kubo et al. (Poster presentation in this conference)
7. S. P. Hirshman and J. C. Whiton, Phys. Fluids **26** pp. 3553-3568 (1983)
8. C. Suzuki, K. Ida, Y. Suzuki et. al, Plasma Phys. Control. Fusion **55** 014016 (7pp) (2013)